



Single cell viability measurements in 3D scaffolds using *in situ* label free imaging by optical coherence microscopy

Joy P. Dunkers*, Young Jong Lee, Kaushik Chatterjee¹

Polymers Division, Material Measurement Laboratory, National Institute of Standards and Technology, Gaithersburg, MD 20899, United States²

ARTICLE INFO

Article history:

Received 28 September 2011

Accepted 22 November 2011

Available online 20 December 2011

Keywords:

Cell viability

Hydrogel

Image analysis

Scaffold

Stem cell

ABSTRACT

The focus on creating tissue engineered constructs of clinically relevant sizes requires new approaches for monitoring construct health during tissue development. A few key requirements are that the technology be *in situ*, non-invasive, and provide temporal and spatial information. In this work, we demonstrate that optical coherence microscopy (OCM) can be used to assess cell viability without the addition of exogenous probes in three-dimensional (3D) tissue scaffolds maintained under standard culture conditions. This is done by collecting time-lapse images of speckle generated by sub-cellular features. Image cross-correlation is used to calculate the number of features the final image has in common with the initial image. If the cells are live, the number of common features is low. The number of common features approaches 100% if the cells are dead. In control experiments, cell viability is verified by the addition of a two-photon fluorescence channel to the OCM. Green fluorescent protein transfected human bone marrow stromal cells cultured in a transparent poly(ethylene glycol) tetramethacrylate hydrogel scaffold is used as the control system. Then, the utility of this approach is demonstrated by determining L929 fibroblast cell viability in a more challenging matrix, collagen, an optical scatterer. These results demonstrate a new technique for *in situ* mapping of single cell viability without any exogenous probes that is capable of providing continuous monitoring of construct health.

Published by Elsevier Ltd.

1. Introduction

There are factors that affect cell viability in tissue engineered (TE) constructs which are not prevalent in healthy tissues and organs *in vivo*. These challenges are magnified because the field is progressing toward constructs of clinically relevant size, which means that these challenges to cell viability are not only mapped temporally, but also spatially. For example, hypoxia is an issue due to the lack of vasculature and is manifested by dead cells toward the construct interior [1,2]. The scaffold itself can have some degree of cytotoxicity which is seen more predominantly in synthetic scaffolds, or in scaffolds with gradients in composition and modulus [3,4]. Mechanical forces generated by the cell or imposed upon the scaffold can also stress the cells and create pockets of dead cells [5,6]. Perhaps the most universal challenge is the need for successful scale-up of existing technologies for commercialization

to be successful. According to Mather et al. [7], this can be accomplished through a thorough system engineering approach where the response of the cells, scaffold, and environment controls can be continuously monitored over time.

Techniques for evaluating cell viability are many and varied, and a thorough review has been presented elsewhere [8,9]. For *in vitro* evaluation of TE constructs, cell viability is usually evaluated through either metabolic activity, cell membrane integrity, morphology, or reproductive assays [4,10]. Most metabolic activity assays (MTT, XTT) are performed on populations of cells and are not practical for spatial discrimination of cell viability. Cell membrane integrity is used as a measure of viability and can be measured colorimetrically or fluorescently, but the fluorescent dyes are the most selective indicators. Commonly used membrane integrity dyes are calcein AM for the presence of live cells and propidium iodide or ethidium bromide for detection of dying or dead cells. In one example of a label free method, a ¹H nuclear magnetic resonance (NMR) spectroscopy study showed that βTC3 cell viability in agarose obtained by taking the total choline NMR peak area averaged over the entire sample can be correlated to viable cells counted by the MTT assay [11]. Most of the above techniques involve end-point measurements such that cells within a given scaffold are not amenable to repeated time-course measurements.

* Corresponding author. Tel.: +1 301 975 6841; fax: +1 301 975 4977.

E-mail address: joy.dunkers@nist.gov (J.P. Dunkers).

¹ Current address: Department of Materials Engineering, Indian Institute of Science, Bangalore 560012, India.

² Official contribution of the National Institute of Standards and Technology; not subject to copyright in the United States.

For hydrogel derived tissue engineered constructs, several factors exist that can complicate the evaluation of cell viability. First, because the cells are constrained, the morphology of live cells can resemble dead cells. Therefore, evaluations based on cell morphology alone without any external probes can be inaccurate. For constructs of clinically relevant sizes, diffusion of fluorescent dye throughout can be problematic in light of the challenges that exist with oxygen and nutrient diffusion [12]. The ability to monitor one particular tissue construct through the entire culture offers several advantages. These include reduction in the number of samples and associated assays and, most importantly, the ability to follow the fate of individual cells. Therefore, strategies to non-invasively monitor long term tissue construct health are being sought.

Optical coherence tomography (OCT) and its variants, including optical coherence microscopy (OCM), are widely known in the areas of clinical imaging as highly effective tools for imaging deep within tissue with maximum spatial resolutions on the order of 1 μm [13]. The technology's impact is too large to review here, and the authors refer the reader to a comprehensive website (www.octnews.org) for the latest advances in the field. OCT's effectiveness for imaging deep within a sample originates from its ability to detect small changes in refractive index. This is accomplished by using interferometric detection of back-reflected light, where a weak signal is amplified by a strong local oscillator. OCT uses the amplified signal to reconstruct weakly reflecting or obscured features, such as cells in natural or synthetic hydrogels. One of the earliest papers demonstrated that OCT could discriminate between cell and scaffold interior [14]. Since then, the application of OCT to image TE constructs has addressed a large number of tissue types and recognized hurdles [15–20].

When imaging using OCT, there are several potential contrast mechanisms that can be used to differentiate live and dead cells. Apoptotic cells are on average smaller than live cells, whereas necrotic cells swell and rupture. Also, shape differences may distinguish live from dying or dead cells. Differences in scattering properties are routinely used to distinguish live and dead cells in flow cytometry by plotting the intensity of light scattered forward and at 90° [21]. Differences in volume averaged optical scattering coefficients between live, necrotic and apoptotic cells pellets have been detected using OCT [22]. If the scaffolding material is not optically transparent, then differences in scattering from cells relative to the material can also serve as a contrast mechanism. However, all these contrast mechanisms require the establishment of size, shape or optical property relationships between the live and dead cells and scaffold *a priori*. Therefore, a contrast mechanism that will distinguish between live and dead cells and is independent of cell type, size, shape is desirable.

Detection of sub-cellular motility using coherence domain digital holography has been exploited as a means to detect live and necrotic cells in rat tumor spheroids [23]. The goal in this work is to map global differences in cell motility throughout the tumor and is not a single cell measurement. This technique is similar to OCT and takes advantage of the information present in the speckle patterns obtained from the sample. For tissue and single cell imaging, speckle originates from sub-cellular features that are below the optical spatial resolution. For live cells, this speckle pattern changes with time as sub-cellular components move whereas dead cells maintain the same time-dependant speckle pattern. This has been demonstrated by plotting the standard deviation of the pixel intensity from a fixed-depth image of a healthy tumor and a tumor fixed using glutaraldehyde as a function of time [23]. As expected, the healthy tumor showed significant variability of speckle intensity at each pixel, whereas the fixed tumor showed no time-dependant intensity change.

Another variant of OCT, optical phase microscopy (OPM) has been used to determine cell viability on flat surfaces and on a fiber

scaffold [24]. In OPM, the phase difference between the reference and sample arms is calculated from the Fourier transform of the spectral data and can then be used to determine absolute vertical displacement within a cell [25]. The displacements are sub-wavelength and can be on the order of 1 nm. In the paper by Bagnaninchi et al., cell viability was measured by calculating the standard deviation of the phase fluctuations for successive scans in the z direction. Live cells had large phase fluctuations whereas dead cells had very little. In OPM, a common path interferometer is necessary to attain the stability necessary to detect minute displacements. Consequently, phase detection is limited by the overlap of the objective axial point spread function for the sample reflection and the common path reference reflection. OPM is a high accuracy technique capable of measuring minute displacements and is designed for imaging at relatively small distances from the reference reflection.

We are interested in developing a technique to quantify cell viability in scaffolds approaching clinical size that is independent of cell morphology. In this work, speckle fluctuation derived from time-lapse optical coherence microscopy images is used to distinguish between live and dead cells in TE constructs. As an independent verification of cell viability, two-photon fluorescence (2pF) is also used to image green fluorescent protein (GFP) transfected human bone marrow stromal cells (hBMSCs) in a transparent synthetic hydrogel. Live cells show active sub-cellular motion and high fluorescence intensity. Dead cells demonstrate virtually no sub-cellular motion and very little or no fluorescence. In the OCM channel, live and dead cells are quantified using an algorithm that calculates the number of features in common from the first to the last of four time-lapse images and compensates for small sample translation between image frames. The OCM and 2pF results are placed into groups of live and dead cells using k-means cluster analysis. Agreement within-cluster assignments between OCM and 2pF are compared. Subcellular motion from a fibroblast L929 cell line in an optically scattering hydrogel, collagen, is also imaged only with OCM. The results are processed similarly to the hBMSC hydrogels.

2. Experimental

2.1. Cell culture

2.1.1. Human bone marrow stromal cells

Passage 3 hBMSCs (20 year old female) transfected with a lentivirus to express hrGFP were obtained from Tulane University Center for Gene Therapy (product no: 5077-GFP) and cultured in α -modification of Eagle's minimum essential medium (Invitrogen, CA) supplemented with 16 volume % of fetal bovine serum (Atlanta Biologics, GA), 2 mM L-glutamine, 100 units/ml penicillin and 100 $\mu\text{g}/\text{ml}$ streptomycin (Invitrogen). Media was refreshed every 3 d–4 d. Passage 6 cells at 80% confluency were used for all experiments.

2.1.2. Mouse fibroblasts

L929 mouse fibroblasts (ATCC, VA) were cultured in Eagle minimum essential medium with Earle's salts and non-essential amino acids (Invitrogen) supplemented with 10 volume % fetal bovine serum (FBS, Gibco, CA), 2 mM L-glutamine (Sigma, MO) and 1 mM sodium pyruvate (Sigma). Media was refreshed every 3 d–4 d. Passage 4 cells at 80% confluency were used for all experiments.

2.2. Hydrogel scaffold preparation

2.2.1. Poly(ethylene glycol) tetramethacrylate scaffold

Poly(ethylene glycol) tetramethacrylate (PEGTM) was prepared from 4-arm poly(ethylene glycol) (PEG, 20 kDa molecular mass,

each arm 5 kDa) as described previously [26]. To prepare PEGTM hydrogels, 3×10^5 cells/ml were suspended in 5% PEGTM solution prepared in 0.1 mol/L phosphate-buffered saline (PBS, Invitrogen) containing 0.05% Irgacure-2959 (Ciba Chemicals) described previously [26]. The solution was transferred to a Telfon® mold covered with a glass slide and cured under a 365 nm lamp for 15 min at (2–3) mW/cm². The mold thickness for both types of scaffolds was about 3 mm. The cells in the hydrogels were cultured overnight before imaging. The CO₂ buffered media was replaced with full culture medium as above prepared with CO₂ independent media (Invitrogen), and the scaffolds were imaged at 25 °C. Control experiments over the course of 3 h showed that live cells under these conditions remained live.

2.2.2. Collagen scaffold

To prepare 3D collagen gels, 8 parts (volume fraction) of 3 mg/mL collagen solution (PureCol, Advanced Biomatrix, 97% bovine collagen type I) was mixed with 1 part of 10 x MEM and the pH was adjusted to 7.4 using 1 mol/L NaOH solution. 2×10^5 cells/mL were suspended in the collagen solution and transferred to 6 well-plates and incubated at 37 °C. Cell medium was added to the gels after 2 h.

2.3. Cell apoptosis

Exposing cells to ultraviolet (A + B) light is known to trigger apoptosis and has been studied extensively [27]. Here, hydrogel encapsulated cells were placed in a class II culture hood and exposed to a 30 W mercury arc lamp (Model Z30T8, GE, NY) for 4 h under aseptic conditions before returning to the incubator. Cells were imaged the following day.

2.4. Spectral-domain optical coherence/two-photon fluorescence microscopy

The spectral-domain optical coherence/two-photon fluorescence microscope (OCM/2pM) was built in collaboration with Distant Focus Corporation (Longmont, CO) and Professor Stephen Boppart (University of Illinois at Urbana-Champaign, Urbana, IL) through a Small Business Innovative Research grant and is similar in function to the microscope described in Vinegoni et al. [28]. A schematic of the OCM/2pM is shown in Fig. 1. The light source is a Ti:Sapphire laser (Mira, Coherent Inc., CA) operating at a center wavelength of 895 nm, bandwidth of 10 nm, and a pulse width of 100 fs pumped with a solid-state laser at 532 nm (Verdi V10, Coherent). A prism pair compressor was placed before the interferometer to pre-compensate the dispersion due to the high numerical aperture objective (XLUMPLFN, 20X, 0.95 NA, 2 mm working distance, Olympus Inc., PA). This infrared long-working distance objective enables imaging deep into the interior of the scaffold.

The broadband (700 nm–1100 nm) non-polarizing beamsplitter cube launches the light into the interferometer and microscope paths. Leading to the upright microscope (Model BX61WI, Olympus Inc., PA) is the x,y scanning galvanometer (Cambridge Technology, MA) and optics for beam expansion. A piezo stage is mounted on the fixed turret for objective movement in z. Samples were placed on a tilt stage fixed onto an x,y translation stage (Model H105 ProScan II, Prior Scientific, MA). A lever on the microscope turret directs reflected laser light either to a charge-coupled device (CCD) camera or to the two-photon fluorescence (2pF) detector. The CCD camera displays the live brightfield and laser spot image, and the

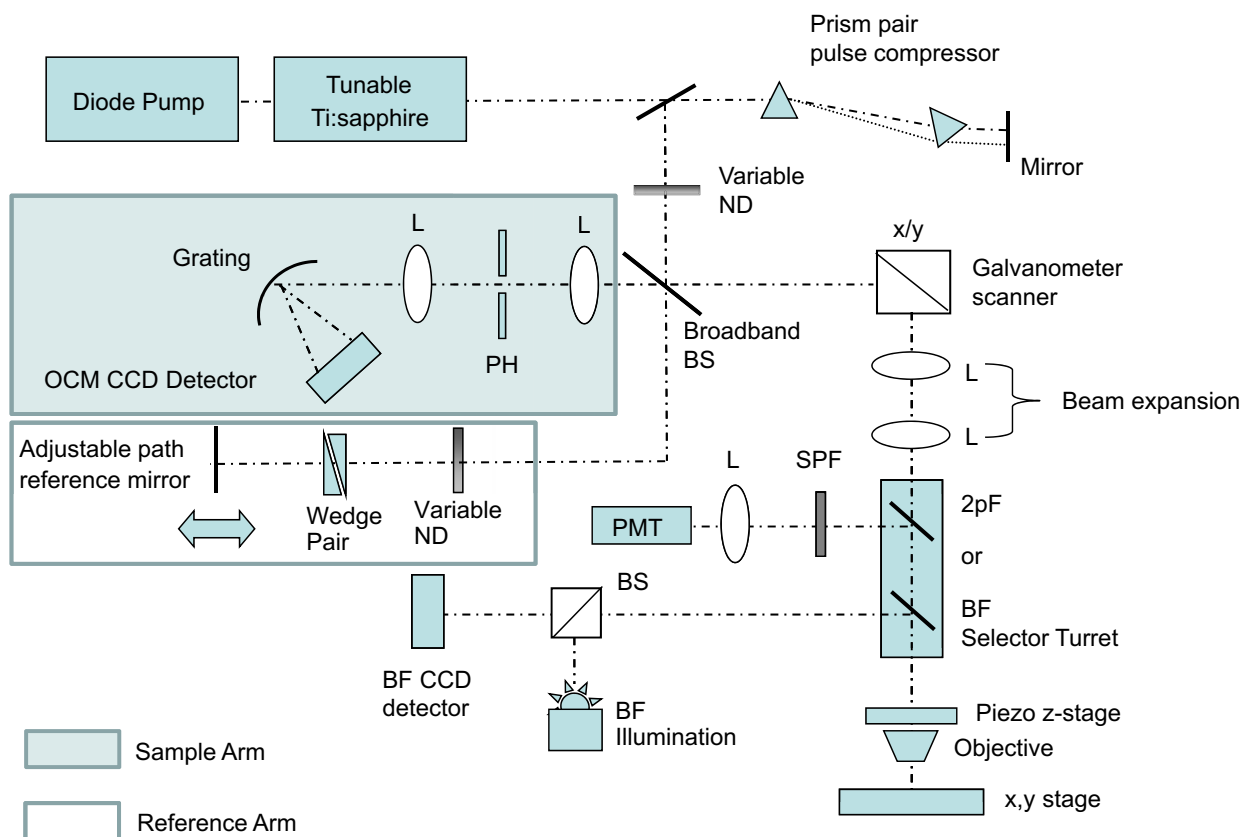


Fig. 1. Optical coherence (OCM)/two-photon fluorescence (2pF) microscope optomechanical diagram. BF: brightfield, BS: beamsplitter, CCD: charge-coupled device, L: lens, ND: neutral density filter, PH: pinhole, PMT: photo-multiplier tube, SPF: short pass filter.

two-photon fluorescence light passes through a focusing lens and a long pass filter before it arrives at a photon counting head (peak quantum efficiency of 40% at 580 nm, Hamamatsu, NJ).

This OCM is designed for spectral-domain detection [29]. A comparison of spectral (SD) and time domain (TD) detection techniques has been presented [30]. Advantages of SD over TD include higher achievable imaging speed, higher dynamic range and more flexibility on source shape. However, SD systems are typically more expensive than TD, involve more intensive signal processing, and require superior vibration isolation. The first element in the interferometer is a variable neutral density filter. OCM detector arm consists of a constant deviation concave monochromator grating (1200 grooves/mm, Newport, CA) and a 1024 pixel, 12 bit charge-coupled device (CCD) camera (Spyder 3, Teledyne DALSA Inc., MA). A telescope with a 5 μm pinhole is placed before the grating to achieve confocality. The reference arm consists of a variable neutral density filter, a glass wedge to match objective dispersion, and a mirror. The total path length in the reference arm is adjusted to match the distance to the sample arm.

OCM lateral resolution was determined by the minimum resolvable pitch for lines on a Metrochip (Ted Pella Inc., CA) microscope calibration target, and was measured to be 0.7 μm . The coherence length of the source, assuming a Gaussian spectral distribution, was 36 μm [31]. The axial resolution (full-width at half-maximum intensity) results from the convolution of the source coherence length and the objective axial point spread function (PSF) [32] and was measured to be 4 μm . The sensitivity of the OCM signal was measured to be -91 dB using the equation $-20 \log(\text{peak intensity}/\text{noise variance})$ on a mirror surface.

Two-photon fluorescence microscopy has a resolution similar to one-photon confocal fluorescence but without the intensity losses associated with the pinhole. Therefore, using 510 nm for the GFP emission wavelength, the lateral resolutions was calculated to be 330 nm. Using the equation below for PSFs 1 AU and above, the axial resolution was calculated to be 1100 nm:

$$\text{FWHM}_{\text{axial}} = \frac{0.88\lambda}{(n - \sqrt{n^2 - \text{NA}^2})}$$

Where $\lambda = 510$ nm, n is refractive index of immersion medium (water = 1.33 at 25 °C), and NA is the numerical aperture of the objective (NA = 0.95).

2.5. Image acquisition and processing

Acquiring simultaneous OCM and 2pF images required balancing the power needs of both techniques. OCM traditionally operates using low power, typically a (<5 mW) whereas higher peak power per unit area is required to excite the non-linear two-photon process. For this work, images were acquired using powers below 600 μW which was well below the damage initiation power [33]. Both channels were acquired at a camera rate of 10 kSamples/s, which corresponded to 20 s per image with a total of four images collected consecutively to create a time-lapse movie in 90 s. The image size was 60 μm at 256×256 pixels. For the OCM, complete spectra were obtained for each pixel in the image and stored in hdf5 format. Using a Matlab custom program, spectra were Fourier transformed, the peak maximum was detected and then used as the intensity value for the corresponding pixel. The intensity of each time-lapse image set was scaled to the maximum intensity for the set of four images. For the 2pF, the fluorescence intensity data was read from the hdf5 file, scaled to the maximum intensity from the image set, and written back out as an image.

2.6. Feature recognition

Subcellular motion was quantified by comparing time-lapse speckle patterns obtained using OCM. This was accomplished using a Matlab code written by David Young (University of Sussex, Brighton, UK) entitled: Image correspondences using cross-correlation [34] and is intended for use in applications where optical flow, stereo disparity or image registration is needed. This program was amended to include a cropping function that will enable the user to select the area of interest. This function is necessary for the L929 and collagen images where the entire image has speckle content. In this work, the time-lapse image set consists for four images. The set of code developed by Young first finds the features by computing local intensity maxima of image 1 using the variance. Then, feature correspondence between the image 1 and image 2 is found using normalized cross-correlation, which means the results are divided by the product of the standard deviations of the image patches to make the result insensitive to the local contrast. A backwards check for consistency is done by finding the image variance in image 2 and then performing the normalized cross-correlation with image 1. Then, only the features common to images 1 and 2 are retained for comparison to image 3. This process is repeated until the last image is used, which in this case is image 4. Then, the feature match (%) is calculated, which is the number of features detected in the last comparison divided by the total number of features in the first comparison. A parametric study was done on the adjustable variables: threshold and feature size. Changing these variables did affect the number of features detected but had little effect on the feature match between two test images. Those cells that retain the speckle pattern between image frames have a high percentage of feature correspondence. Likewise, those cells whose speckle pattern changes dramatically between frames have a low percentage of feature correspondence.

For the fluorescence images, the normalized fluorescence intensity was calculated by first taking the average intensity of a region of interest (ROI) bounding the cell. This value was divided by the average intensity of the ROI in the background. For images with low fluorescence where the cell boundaries could not be easily distinguished, the ROI was created from the corresponding OCM image.

3. Results and discussion

To test our OCM method for measuring cell viability, control samples of GFP transfected hBMSCs in PEGTM hydrogels were fabricated and exposed to either “untreated” or “UV” conditions as detailed in the experimental section. The “untreated” samples were handled using standard cell culture protocols to maintain living cells. The hydrogels were subjected to ultraviolet 285 nm light to intentionally kill the cells in the “UV” samples. Cells were randomly selected at different lateral and depth locations for imaging. We have not determined whether apoptosis or necrosis occurred, and that assignment is not within the scope of this work. Therefore, cells will be referred to either as “live” or “dead”. These assignments were initially done qualitatively by observing characteristics of the OCM speckle pattern and the 2pF. Brightfield (BF), OCM and 2pF images of live cells in the untreated condition and dead cells subjected to UV are shown in Fig. 2. The BF (A, E, I) and 2pF (D, H, L) images are static whereas the OCM images are the first and last frames of time-lapse movies that show the speckle behavior from sub-cellular feature scattering. The cells in Fig. 2(A–D) are live because of the active sub-cellular motion in the OCM channel as manifested by differences in the speckle pattern in Fig. 2B and C and robust GFP intensity (Fig. 2D). The BF (2A) image displays low contrast relative to its hydrogel background. In contrast, the UV

treated cell shown in Fig. 2F and G shows virtually identical speckle patterns and virtually no 2pF (Fig. 2H). Using the same illumination as the live cell, the dead cell in Fig. 2E has a higher back reflectance. In live cells, the fluorophore reporter resides in the cytoplasm. During cell death, the fluorophore exits the cell and fluorescence is diminished or completely lost [35]. To confirm that fluorescence is lost through a compromised membrane and not through photobleaching, the hBMSC cells were fixed with 3.7 vol. % formaldehyde in PBS to maintain cell membrane integrity and imaged with 2pF. The fluorescence was retained in the fixed cells (data not shown). To serve as an additional comparison for the optical contrast mechanisms seen in live and dead cells, Fig. 2(I–L) shows one live and one dead cell in close proximity. As expected, the dead cell has a higher reflectance in the BF channel than the live cell. A clear demonstration of the differences in speckle fluctuation is seen between Fig. 2J and K. Again, the speckle pattern is different for the live cell (left) whereas the major speckle features are identical for the dead cell (right). The corresponding bright fluorescence from the live hBMSC (left of center) in Fig. 2L is contrasted by the lack of fluorescence in the dead. These OCM images provide a qualitative illustration of cell viability without exogenous fluorophores, and the 2pF offers complementary information. However, quantifying the changing OCM speckle pattern is necessary for several reasons. First, because of the low modulus of the hydrogel (11 kPa [26]) some cells may move slightly between frames. Quantifying the dynamic speckle pattern allows only true changes in sub-cellular motion to be tracked and not speckle pattern shifting due to construct translation. Second, it offers a direct correlation between OCM and 2pF. Lastly, image speckle quantification allows groups to be established for the live and dead assignments.

The sub-cellular, dynamic speckle pattern from the OCM channel was quantified using the image cross-correlation program. In Fig. 3, the OCM feature match is plotted against the log of the 2pF

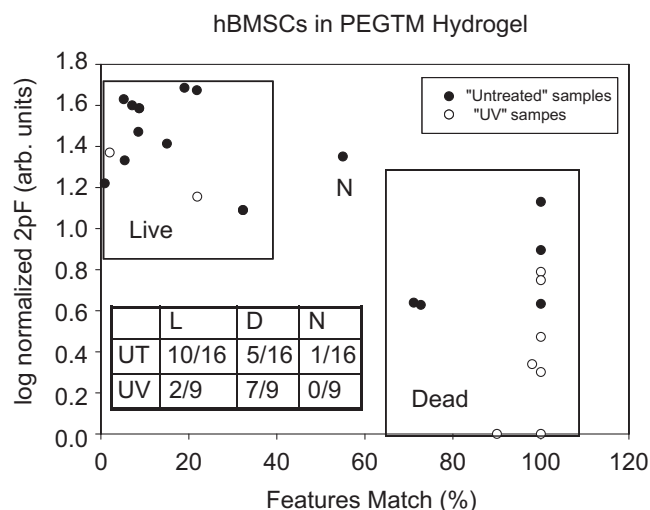


Fig. 3. Scatter plot of 2pF intensity versus percent feature match to show correlations between the data sets. Generally there is good discrimination between viable and non-viable cells, and qualitative assignments of live and dead cells are shown within the boxes. The inset table shows the number of cells for each viability assignment out of the total number of cells for each condition. UT: untreated, UV: UV treated, L: live, D: dead, N: not assigned.

intensity. The log of the fluorescence intensity was used because the live cell fluorescence did exhibit scatter but was almost always above a threshold value while dead cell fluorescence was mostly below a threshold value. It can be seen from this figure that very good agreement in live/dead assignments exists between both techniques. Cells that were live clustered in the upper left part of the graph (high 2pF, low feature matching) while dead cells

Images of hBMSCs in PEGTM

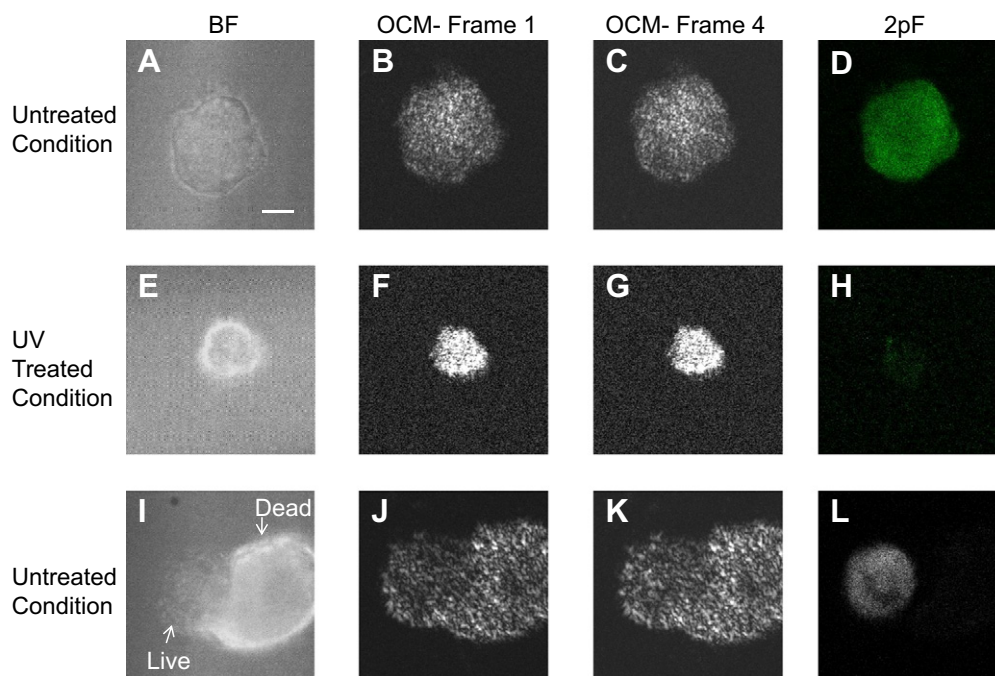


Fig. 2. BF (A, E, I), OCM frame 1 (B, F, J), OCM frame 4 (C, G, K), and 2pF (D, H, L) images of a live cell in the untreated condition (A to D), dead cell exposed to UV (E to H), and co-located live and dead cell (I to L) in the untreated condition. Live cells have active sub-cellular motion as manifested by differences in the speckle pattern between OCM frame 1 and frame 4 (70 s later) and robust fluorescence. Dead cells have minimum sub-cellular motion and little or no speckle pattern differences between OCM frames and low or no fluorescence. Scale bar: 10 μm for all images.

clustered toward the lower right (low 2pF, high feature matching). The inset table shows that about 31% of the cells (5/16) that were present in the “untreated” sample were in fact dead. This is not surprising, considering that after 1 d culture, viable MC3T3 cells ranged from about (45–65)% in a PEG-dimethacrylate hydrogel [4] and 55% for hBMSCs in 11 kPa PEGTM hydrogels [26]. The cell not within either box (N column in table) can be categorized as live from the 2pF results but had very weak OCM speckle intensity which biased the feature match computation. In addition, the table shows that both techniques detect two live cells in a sample that was exposed to UV. To quantify how well the OCM and 2pF results agree in determining whether a cell is “live” or “dead”, cluster analysis was performed.

Cells were partitioned into “live” or “dead” groups using k-means cluster analysis, a function in Matlab® (Mathworks, MA), where k is the number of groups into which the data is to be partitioned. In this case, $k = 2$. This iterative partitioning function minimizes the sum, over all clusters, of the within-cluster sums of point-to-cluster-centroid distances, where the distances to the centroid from each point are measured by the squared Euclidean distance. The cluster analysis in Fig. 4A reveals 12 live cells out of a total of 25, and the live cells have a feature match under 40%, while the 13 remaining dead cells have a feature match above 55%.

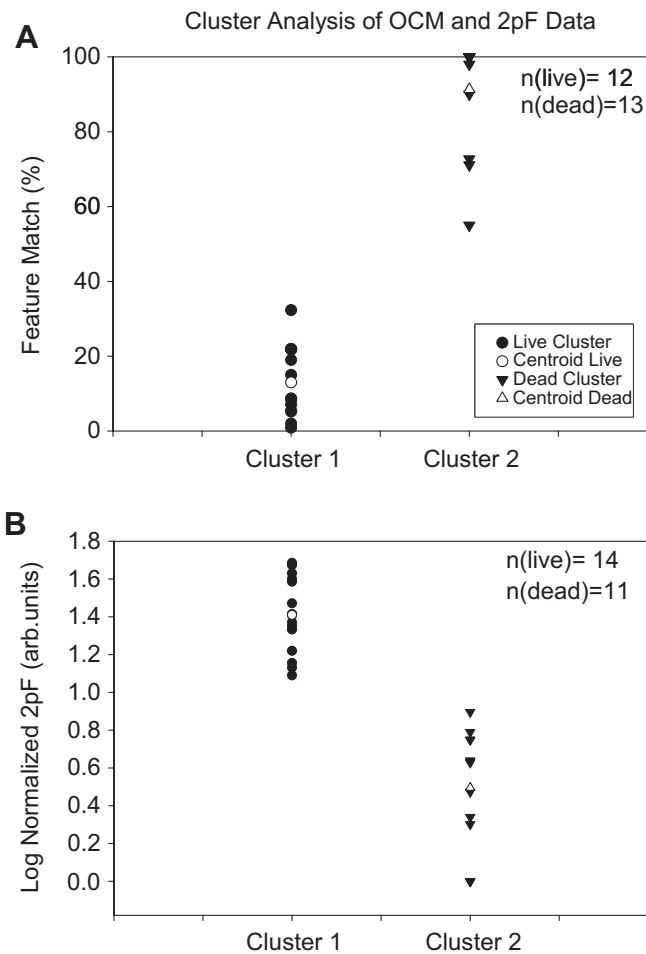


Fig. 4. Cluster analysis of the hBMSC OCM (A) and 2pF (B) data showing the distribution of live and dead assignments from the centroid. For the OCM, there is an even distribution of values around the centroid for the live cells whereas for the dead cells the centroid value is near 90% with a handful of values 80% and below. For the 2pF, there is even distribution of fluorescence intensity around both centroids. The n values reflect the total number of live and dead cells for each cluster.

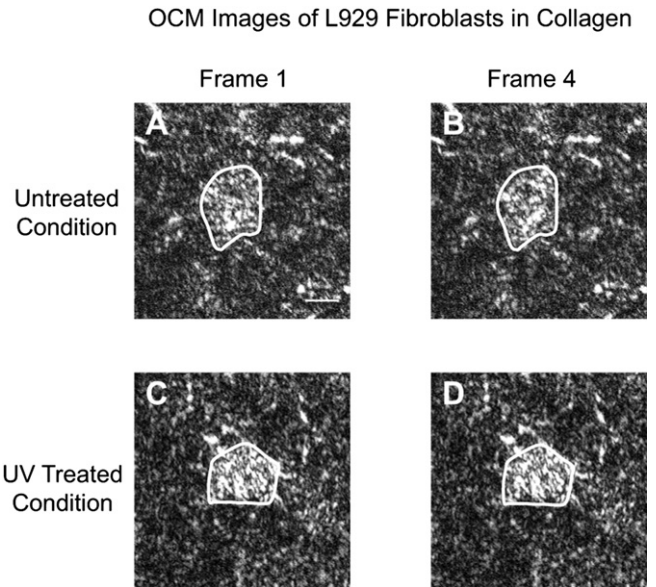


Fig. 5. OCM frame 1 (A, C) and frame 4 (B, D) images of a live cell in the untreated condition (A, B), dead cell exposed to UV (C, D). Live cells have active sub-cellular motion as manifested by differences in the speckle pattern between OCM frame 1 and frame 4 (70 s later). Dead cells have minimum sub-cellular motion and little or no speckle pattern differences between OCM frames. Approximate cell outlines are drawn for clarity. Scale bar: 10 μ m for all images.

For the 2pF, 14 cells were also identified to be live while 11 were dead, with a threshold value of 1.0 to delineate between live and dead cells. This cluster analysis reveals very good agreement in cell viability identification between the OCM and 2pF results (23/25 cells). The viability assignments that did not agree were the outlier datapoint seen in Fig. 3 (OCM = 55%, 2pF = 1.4) and a dead cell that had fluorescence values slightly above the threshold (OCM = 100%, 2pF = 1.1). In these control experiments, the ability of OCM to discriminate between live or dead cells has been verified using another cell viability probe, green fluorescent protein.

Next, OCM was used to determine cell viability without exogenous probes in a collagen gel, a naturally derived scaffold.

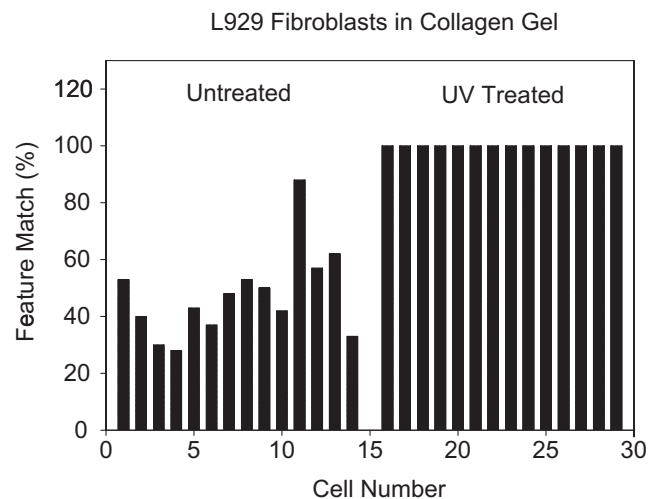


Fig. 6. Percent feature match for L929 cells in collagen for untreated and UV conditions from the four time-lapse OCM images. Note that cell 11 is the only dead cell in the untreated sample, whereas for the UV treated sample all cells were dead with feature matches at 100%.

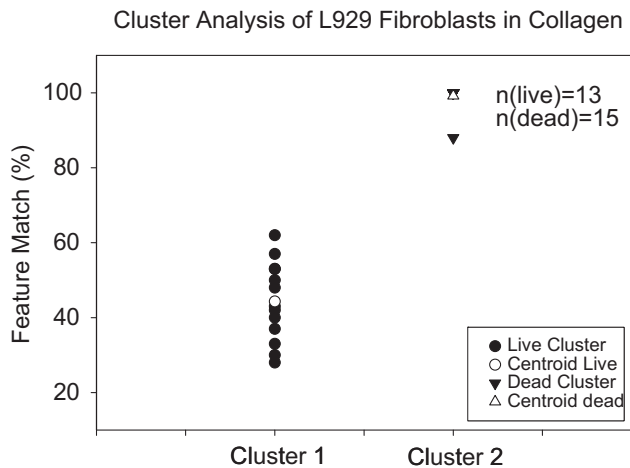


Fig. 7. Cluster analysis of the L929 OCM data showing the distribution of the live and dead assignments from the centroid. There is clear discrimination between live and dead cells.

Collagen was used because it poses additional challenges to our method since it is an optical scatterer. Live hBMSCs assume an elongated spindle morphology in the 3D collagen gels (not shown) that is easily visualized in brightfield microscopy. We used L929 fibroblasts as a model cell line to encapsulate in collagen gels because they do not spread. Therefore, it is difficult to discriminate visually between live and dead cells in the scaffolds based on cell morphology. OCM images of live (untreated condition) and dead (UV treated condition) cells from frame 1 (A, C) and frame 4 (B, D) of the time-lapse movies are shown in Fig. 5. (BF images were not shown due to the very low contrast between cells and collagen matrix). These images are notably different from the hBMSCs in PEG hydrogel since the collagen itself is an optical scatterer and contributes to the features seen in the image. In this figure, outlines are drawn around each cell to aid in identification. In Fig. 5(A, B), the speckle pattern is different between the two frames, indicating that the cell is live. Note that the speckle from the collagen matrix does not change between Fig. 5A and B or C and D. Conversely, the sub-cellular features of frame 1 (Fig. 5C) and frame 4 (Fig. 5D) of the UV treated condition are virtually identical, indicating no sub-cellular motion in a cell that is likely dead.

Fig. 6 displays the OCM image correlation results for the L929 fibroblast samples maintained under untreated and UV treated culture conditions. For the live samples, feature matching was on average higher than for the hBMSCs in the clear PEGTM hydrogel because of overlapping static feature contributions from the collagen. This occurs because of the inability of the cropping routine in the feature correlation program to crop the exact outline of the cell. The viability of the L929s is much higher than the hBMSCs, with only one cell at position 11 indicating dead for the untreated culture conditions. As expected, in the samples where the cells were intentionally killed, the feature match was 100% in all cells sampled. The k-means cluster analysis shown in Fig. 7 shows a clear distinction between the live and dead cells, with more scatter in the feature match for the live cells.

Thus, the OCM technique presented here offers a non-invasive, label free, *in situ* imaging of cell viability in 3D tissue scaffolds. A scaffold can be mapped to examine spatial distribution of viable cells in 3D. In addition, since the technique is non-destructive and non-invasive, a scaffold can be imaged repeatedly to generate a temporo-spatial map of viable cells in TE scaffolds, provided aseptic conditions are also maintained during OCM.

4. Conclusions

In this work, we demonstrate a new technique for *in situ*, three-dimensional measurement of single cell viability without exogenous probes for scaffold thicknesses approaching clinical relevance. We have shown that cell viability can be mapped spatially in hydrogel samples that are several millimeters in thickness by using time-lapse imaging of sub-cellular speckle with optical coherence microscopy. In the hBMSC control hydrogels, live and dead assignments were verified by an independent measure of viability, green fluorescent protein. The number of live and dead cells can be quantified using algorithms that analyze common features in time-lapse images and compensate for small translations of the hydrogel sample. There was good agreement in viability assignments between images collected from the optical coherence and two-photon fluorescence channels. We also demonstrated that cell viability could be determined in optically scattering hydrogels. These results validate a new method for measurement of cell viability in tissue scaffolds that is single cell, *in situ*, non-invasive, quantitative, spatially resolved and amenable to continuous monitoring.

Acknowledgments

The authors would like to thank Carl Simon from the Biomaterials Group for his support and advice regarding this work. The authors would also like to acknowledge John Elliott from the Biochemical Sciences division for his cell biology advice and recommendations.

Certain equipment, instruments or materials are identified in this paper in order to adequately specify the experimental details. Such identification does not imply recommendation by the NIST nor does it imply the materials are necessarily the best available for the purpose.

References

- [1] Demol J, Lambrechts D, Geris L, Schrooten J, Van OH. Towards a quantitative understanding of oxygen tension and cell density evolution in fibrin hydrogels. *Biomaterials* 2011;32(1):107–18.
- [2] Volkmer E, Drosse I, Otto S, Stangelmayer A, Stengele M, Kallukalam BC, et al. Hypoxia in static and dynamic 3D culture systems for tissue engineering of bone. *Tissue Eng Part A* 2008;14(8):1331–40.
- [3] Bryant SJ, Nuttelman CR, Anseth KS. Cytocompatibility of UV and visible light photoinitiating systems on cultured NIH/3T3 fibroblasts *in vitro*. *J Biomat Sci Polym Ed* 2000;11(5):439–57.
- [4] Chatterjee K, Lin-Gibson S, Wallace WE, Parekh SH, Lee YJ, Cicerone MT, et al. The effect of 3D hydrogel scaffold modulus on osteoblast differentiation and mineralization revealed by combinatorial screening. *Biomaterials* 2010;31(19):5051–62.
- [5] Berry CC, Shelton JC, Lee DA. Cell-generated forces influence the viability, metabolism and mechanical properties of fibroblast-seeded collagen gel constructs. *J Tissue Eng Regen M* 2009;3(1):43–53.
- [6] Breuls RG, Bouten CV, Oomens CW, Bader DL, Baaijens FP. Compression induced cell damage in engineered muscle tissue: an *in vitro* model to study pressure ulcer aetiology. *Ann Biomed Eng* 2003;31(11):1357–64.
- [7] Mather ML, Morgan SP, Crowe JA. Meeting the needs of monitoring in tissue engineering. *Regen Med* 2007;2(2):145–60.
- [8] Park JC, Hwang YS, Suh H. Viability evaluation of engineered tissues. *Yonsei Med J* 2000;41(6):836–44.
- [9] Stoddart MJ. Cell viability assays: introduction. *Methods Mol Biol* 2011;740:1–6.
- [10] Doroski DM, Brink KS, Temenoff JS. Techniques for biological characterization of tissue-engineered tendon and ligament. *Biomaterials* 2007;28(2):187–202.
- [11] Stabler CL, Long RC, Sambanis A, Constantinidis I. Noninvasive measurement of viable cell number in tissue-engineered constructs *in vitro*, using ¹H nuclear magnetic resonance spectroscopy. *Tissue Eng* 2005;11(3–4):404–14.
- [12] Malda J, Klein TJ, Upton Z. The roles of hypoxia in the *in vitro* engineering of tissues. *Tissue Eng* 2007;13(9):2153–62.
- [13] Fercher AF. Optical coherence tomography – development, principles, applications. *Z Med Phys* 2010;20(4):251–76.
- [14] Dunkers J, Cicerone M, Washburn N. Collinear optical coherence and confocal fluorescence microscopies for tissue engineering. *Opt Express* 2003;11(23):3074–9.

- [15] Chen CW, Betz MW, Fisher JP, Paek A, Chen Y. Macroporous hydrogel scaffolds and their characterization by optical coherence tomography. *Tissue Eng Part C Methods* 2011;17(1):101–12.
- [16] Jia Y, Bagnaninchi PO, Yang Y, Haj AE, Hinds MT, Kirkpatrick SJ, et al. Doppler optical coherence tomography imaging of local fluid flow and shear stress within microporous scaffolds. *J Biomed Opt* 2009;14(3):034014.
- [17] Patterson J, Stayton PS, Li X. In situ characterization of the degradation of PLGA microspheres in hyaluronic acid hydrogels by optical coherence tomography. *IEEE T Med Imaging* 2009;28(1):74–81.
- [18] Smith LE, Bonesi M, Smallwood R, Matcher SJ, MacNeil S. Using swept-source optical coherence tomography to monitor the formation of neo-epidermis in tissue-engineered skin. *J Tissue Eng Regen M* 2010;4(8):652–8.
- [19] Wang Z, Pan H, Yuan Z, Liu J, Chen W, Pan Y. Assessment of dermal wound repair after collagen implantation with optical coherence tomography. *Tissue Eng Part C Methods* 2008;14(1):35–45.
- [20] Gomez-Lara J, Brugaletta S, Diletti R, Garg S, Onuma Y, Gogas BD, et al. A comparative assessment by optical coherence tomography of the performance of the first and second generation of the everolimus-eluting bioresorbable vascular scaffolds. *Eur Heart J* 2011;32(3):294–304.
- [21] Darzynkiewicz Z, Juan G, Li X, Gorczyca W, Murakami T, Traganos F. Cytometry in cell necrobiology: analysis of apoptosis and accidental cell death (necrosis). *Cytometry* 1997;27(1):1–20.
- [22] van der Meer FJ, Faber DJ, Aalders MC, Poot AA, Vermees I, van Leeuwen TG. Apoptosis- and necrosis-induced changes in light attenuation measured by optical coherence tomography. *Lasers Med Sci* 2010;25(2):259–67.
- [23] Jeong K, Turek JJ, Nolte DD. Volumetric motility-contrast imaging of tissue response to cytoskeletal anti-cancer drugs. *Opt Express* 2007;15(21):14057–64.
- [24] Bagnaninchi PO, Holmes C, Drummond N, Daoud J, Tabrizian M. Two-dimensional and three-dimensional viability measurements of adult stem cells with optical coherence phase microscopy. *J Biomed Opt* 2011;16(8):086003.
- [25] Joo C, Akkin T, Cense B, Park BH, de Boer JF. Spectral-domain optical coherence phase microscopy for quantitative phase-contrast imaging. *Opt Lett* 2005;30(16):2131–3.
- [26] Parekh SH, Chatterjee K, Lin-Gibson S, Moore NM, Cicerone MT, Young MF, et al. Modulus-driven differentiation of marrow stromal cells in 3D scaffolds that is independent of myosin-based cytoskeletal tension. *Biomaterials* 2011;32(9):2256–64.
- [27] Kulms D, Schwarz T. Molecular mechanisms involved in UV-induced apoptotic cell death. *Skin Pharmacol Appl* 2002;15(5):342–7.
- [28] Vinegoni C, Ralston T, Tan W, Luo W, Marks DL, Boppart SA. Integrated structural and functional optical imaging combining spectral-domain optical coherence and multiphoton microscopy. *Appl Phys Lett* 2006;88(5):053901–3.
- [29] Morgner U, Drexler W, Kartner FX, Li XD, Pitris C, Ippen EP, et al. Spectroscopic optical coherence tomography. *Opt Lett* 2000;25(2):111–3.
- [30] Lindner MW, Andretzky P, Kiesewetter F, Hausler G. Spectral radar: optical coherence tomography in the Fourier domain. In: Bouma B, Tearney G, editors. *The handbook of optical coherence tomography*. New York: Marcel Dekker, Inc; 2002. p. 335–57.
- [31] Fujimoto JG. Optical coherence tomography: introduction. In: Bouma B, Tearney G, editors. *The handbook of optical coherence tomography*. New York: Marcel Dekker, Inc; 2002. p. 6.
- [32] Wang HW, Izatt JA, Kulkarni MD. Optical coherence microscopy. In: Bouma B, Tearney G, editors. *The handbook of optical coherence tomography*. New York: Marcel Dekker, Inc; 2002. p. 281–3.
- [33] Konig K, So PT, Mantulin WW, Gratton E. Cellular response to near-infrared femtosecond laser pulses in two-photon microscopes. *Opt Lett* 1997;22(2):135–6.
- [34] Available from: URL: <http://www.mathworks.com/matlabcentral/fileexchange/authors/41349>. 2011.
- [35] Strebel A, Harr T, Bachmann F, Wernli M, Erb P. Green fluorescent protein as a novel tool to measure apoptosis and necrosis. *Cytometry* 2001;43(2):126–33.